

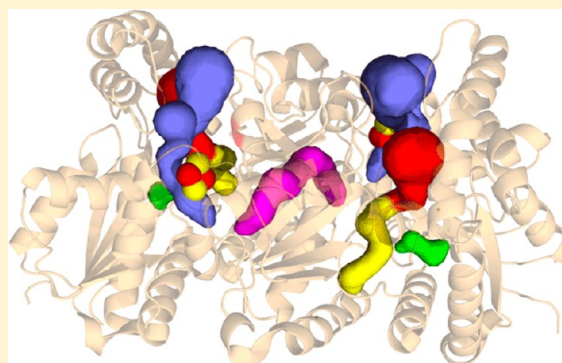
# Identification and Characterization of Solvent-Filled Channels in Human Ferrochelatase

Amy E. Medlock,\* Wided Najahi-Missaoui,<sup>†</sup> Teresa A. Ross,<sup>‡</sup> Tamara A. Dailey, Joseph Burch, Jessica R. O'Brien, William N. Lanzilotta, and Harry A. Dailey

Biomedical and Health Sciences Institute, Department of Biochemistry and Molecular Biology, University of Georgia, Athens, Georgia 30602, United States

## Supporting Information

**ABSTRACT:** Ferrochelatase catalyzes the formation of protoheme from two potentially cytotoxic products, iron and protoporphyrin IX. While much is known from structural and kinetic studies on human ferrochelatase of the dynamic nature of the enzyme during catalysis and the binding of protoporphyrin IX and heme, little is known about how metal is delivered to the active site and how chelation occurs. Analysis of all ferrochelatase structures available to date reveals the existence of several solvent-filled channels that originate at the protein surface and continue to the active site. These channels have been proposed to provide a route for substrate entry, water entry, and proton exit during the catalytic cycle. To begin to understand the functions of these channels, we investigated in vitro and in vivo a number of variants that line these solvent-filled channels. Data presented herein support the role of one of these channels, which originates at the surface residue H240, in the delivery of iron to the active site. Structural studies of the arginyl variant of the conserved residue F337, which resides at the back of the active site pocket, suggest that it not only regulates the opening and closing of active site channels but also plays a role in regulating the enzyme mechanism. These data provide insight into the movement of the substrate and water into and out of the active site and how this movement is coordinated with the reaction mechanism.



Heme is an essential molecule for most organisms and is a cofactor for proteins involved in a number of cellular processes, including aerobic respiration, carbohydrate and lipid metabolism, nucleic acid processing, and cellular signaling.<sup>1–3</sup> Within eukaryotes, the biosynthetic pathway is conserved after the synthesis of the first committed intermediate, 5-amino-levulinate (ALA), while in prokaryotes, significant differences are found at several steps. However, among all organisms, the terminal step of the pathway, chelation of ferrous iron into the protoporphyrin ring by the enzyme ferrochelatase, is conserved. The two best studied ferrochelatase proteins are from the bacterium *Bacillus subtilis* and humans. Both of these enzymes have been well characterized kinetically, spectroscopically, and structurally. Despite having sequences that are <10% identical, they have highly similar tertiary structure and substrate specificities. The *B. subtilis* protein is a soluble monomer that probably functions in vivo as part of a multienzyme complex,<sup>4</sup> while the human enzyme is a homodimer that is associated with the inner mitochondrial membrane.<sup>5,6</sup> Because of the reactive nature of the substrates and product of the ferrochelatase reaction, both substrate entry and product release must be highly coordinated processes in vivo to prevent cytotoxicity. Knowledge of the mechanisms by which this occurs in higher animals is critical to our understanding of diseases resulting from defects in iron, porphyrin, and/or heme metabolism.

Primarily on the basis of structural studies of *B. subtilis* ferrochelatase with and without the bound tight-binding competitive inhibitor *N*-methylmesoporphyrin, it was suggested that ferrochelatase functioned as a relatively rigid molecule with an active site mouth within which substrate porphyrin bound and distorted to allow metal insertion. However, the determination of the structure of human ferrochelatase with the porphyrin substrate bound<sup>8</sup> revealed that the enzyme is quite dynamic and that the “open” active site mouth of the substrate free enzyme (Figure 1A) closes to tightly bind and distort the porphyrin macrocycle. In this conformation [the so-called “closed” conformation (Figure 1B)], the bound porphyrin occupies a spatial position in the enzyme that is distinct from that observed for *N*-methylmesoporphyrin in the *B. subtilis* enzyme.<sup>9,10</sup> The closed conformation has been observed in the substrate-bound form of human ferrochelatase and in one subunit of the *Saccharomyces cerevisiae* ferrochelatase.<sup>11</sup> Additionally, structures of the product (heme)-bound enzyme revealed a third conformational variant of human ferrochelatase [the so-called “release” conformation (Figure 1C)].<sup>12,13</sup> In this form, a structurally conserved  $\pi$ -helix that

Received: May 7, 2012

Revised: June 12, 2012

Published: June 19, 2012



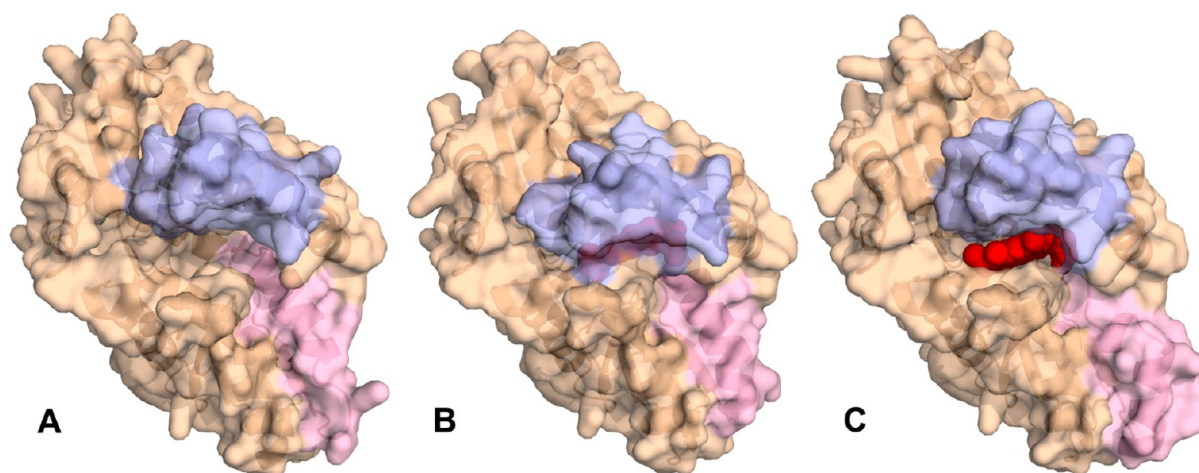


**Figure 1.** Surface and cartoon representations of the three conformations observed for the human ferrochelatase dimer. (A) Open conformation as observed in the R115L variant [Protein Data Bank (PDB) entry 2HRC]. (B) Closed conformation as observed in the substrate-bound E343K variant (PDB entry 2QD1). (C) Release conformation from the heme-bound F110A variant (PDB entry 2QD2). The bound porphyrin and heme are shown in the active site as spheres. The surface of the upper lip region is colored purple and the  $\pi$ -helix pink.

forms part of one wall of the active site<sup>14</sup> is found to be partially unwound, extending away from the active site pocket. Consistent with kinetic studies demonstrating that the reaction proceeds in an ordered fashion<sup>15–17</sup> with the slowest step in the reaction being an event occurring after chelation, it has been proposed that the rate-limiting step is most likely product release<sup>18</sup> and involves the unwinding of the  $\pi$ -helix.<sup>12,13</sup>

Interestingly, each of the three enzyme conformations (i.e., open, closed, and release) possesses a distinct surface contour and surface potential around the mouth region of the enzyme. These catalytically distinct conformational states have been suggested to provide different surfaces upon which multiple protein partners may bind during a complete catalytic cycle.<sup>13,19</sup> Not surprisingly, the structural changes observed among the three conformations are not limited to the surface of the protein. The spatial orientation and hydrogen bonding networks of active site residue side chains have also been observed to vary among the three conformational states.<sup>8,13,20</sup> Given the extent of the conformational changes that occur upon going from the open to closed and finally the release state, any complete catalytic model must embrace and explain the significant protein structural rearrangements that have been observed.

Ferrochelatase, as an enzyme that is bound to the matrix side of the inner mitochondrial membrane, must obtain both substrates (porphyrin and iron) and release product (heme) across the inner mitochondrial membrane. Hints at how these processes may occur lie in the structural differences seen in the three known conformational states of human ferrochelatase. While conformational changes during catalysis of human ferrochelatase are now well accepted, the fact that all current structures of *B. subtilis* ferrochelatase, including those with the bound inhibitors *N*-methylmesoporphyrin and 2,4-disulfonate-deuteroporphyrin,<sup>9,10</sup> are of the open (substrate free) form of the enzyme has led to speculation that the bacterial and eukaryotic ferrochelatases somehow differ in their catalytic mechanism.<sup>21</sup> However, no structure of the bacterial enzyme with either bound porphyrin substrate or heme has been characterized to date. Of note with respect to the current discussion is the H240A human ferrochelatase structure presented herein (below) in which the presence of a  $Mg^{2+}$

atom was observed coordinated via water molecules to several residues of the conserved  $\pi$ -helix and a backbone atom of K304 (Figure S1 of the Supporting Information).  $Mg^{2+}$  ions in this position have been observed in most *B. subtilis* structures, and it is reported to be required for crystal formation of the *B. subtilis* enzyme.<sup>22</sup> We suggest that the presence of  $Mg^{2+}$  interacting with the  $\pi$ -helix probably stabilizes the protein in the open conformation, which may explain why only this conformation of the *B. subtilis* enzyme has been observed. A definitive answer to the proposal that the bacterial enzyme operates via a mechanism different from that of the human enzyme must await the availability of structures of that protein with bound protoporphyrin and product.

In addition to the incomplete understanding of the precise role of many active site residues, information about the mechanism of iron entry as well as steps involved in product exit is lacking. Recent evidence that the mitochondrial inner membrane iron transporter mitoferrin 1 and ferrochelatase physically interact<sup>19</sup> suggests that iron transported across the membrane may be donated directly from mitoferrin 1 to a surface of ferrochelatase. How the iron transits from the outer surface of ferrochelatase to the active site is unknown. However, a recent proposal that the extended  $\pi$ -helix may stretch back into the matrix space and pull iron into the active site<sup>21,23</sup> is clearly untenable given the spatial orientation of human ferrochelatase in the inner mitochondrial membrane. We propose that solvent-filled channels in human ferrochelatase that originate at the surface and terminate in the active site may serve as the entry route for substrate iron and/or as aqueducts that function in substrate binding or product release.<sup>20</sup> The work presented herein characterizes several stable solvent-filled channels that exist in human ferrochelatase. Special consideration is given to the side chain of residue F337 because structural data indicate that it is involved in control of the gating of two active site channels as well as in regulating changes in the resting state hydrogen bonding network during catalysis in distinct regions of the active site.

## ■ MATERIALS AND METHODS

**Mutagenesis, Protein Expression and Purification, and Assessment of Enzyme Activity.** All variants were

created using the QuikChange site-directed mutagenesis protocol (Agilent, Santa Clara, CA). Tunnel variants were constructed in the R115L background.<sup>5</sup> Two exceptions to this were the F337R variant and the S197C/F110A double variant, which were constructed in the wild-type background. Expression and purification of all variants were conducted as previously described.<sup>5,24,25</sup> The enzyme activity of each variant was assessed first by rescue of a ferrochelatase deficient strain of *Escherichia coli* ( $\Delta hemH$ ).<sup>26,27</sup> Following rescue of  $\Delta hemH$ , variant ferrochelatases were assayed using the continuous direct spectroscopic method.<sup>28</sup>

***S. cerevisiae*  $\Delta hem15$  Complementation and Heme Quantitation.** All wild-type and variant ferrochelatase genes were cloned into low-copy number yeast shuttle vector pRS316 (gift from W. K. Schmidt, University of Georgia) behind a 350 bp fragment that contained the *S. cerevisiae* ferrochelatase promoter and targeting sequence. Human ferrochelatase variants were constructed by using the wild-type human ferrochelatase/pRS316 vector as a template and QuikChange mutagenesis (Agilent). Wild-type *S. cerevisiae* strain DY1457 (*MAT $\alpha$* , *ade6*, *can1*, *his3*, *leu2*, *trp1*, *ura3*) and a ferrochelatase deficient strain ( $\Delta hem15$ )<sup>29</sup> (gifts from J. Kaplan and R. J. Crisp, University of Utah, Salt Lake City, UT) were utilized. Cells were grown at 30 °C with vigorous shaking in complete medium (1% yeast extract and 1% bacto-peptone) with 3% glycerol as a carbon source. In the  $\Delta hem15$  strain lacking the ferrochelatase-encoded plasmid, the medium was supplemented with 1.5 mg/mL hemin (Sigma, St. Louis, MO) made fresh in 0.1 N NaOH and filter-sterilized. Competent  $\Delta hem15$  cells were made and transformed with wild-type and variant ferrochelatase pRS316 constructs using the Frozen-EZ Yeast Transformation II kit (Zymo Research, Orange, CA). Cells were plated and selected on CM-Uracil with 3% glycerol. The whole cell cytochrome content was estimated using a modified version of the previously described pyridine hemochromagen method.<sup>30</sup> Yeast cells harboring the ferrochelatase variants were grown and harvested in midlog phase. Cells were spheroplasted using Zymolyase (MP Biomedicals, Solon, OH). The total protein content of spheroplasts was measured using the BCA assay (Pierce, Rockford, IL). Duplicate samples were used in the hemochromagen assays. The 550 nm peak and the total cellular protein concentration were used to calculate the total amount of cytochromes *b* and *c* because they represent the major heme pools.

**Crystallization, Data Collection, Model Building, Refinement, and Coordinates.** Protein for crystallization was prepared as previously described.<sup>8,13</sup> All crystals were grown using the hanging drop method by mixing 2  $\mu$ L of freshly prepared enzyme with an equivalent amount of well solution, followed by incubation at 18 °C. The EasyXtal Crystal support (Qiagen, Valencia, CA) was used for crystallization, and each well contained 500  $\mu$ L of the precipitating solution. Crystals typically formed in 2–5 days. Crystals for the H240A variant were obtained using a well solution of 0.2 M magnesium chloride, 0.1 M Bis-Tris (pH 6.5), and 25% PEG 3350. Crystals for the F337R and S197C/F110A variants were obtained using the precipitating solution containing 0.1 M Bis-Tris (pH 6.5), 0.05 M ammonium sulfate, and a range of concentrations of pentaerythritol ethoxylate (15/4 EO/OH) varying from 20 to 35%. The H240A crystals were soaked in a stepwise fashion (2.5% increments) in mother liquor containing increasing concentrations of glycerol to a final concentration of 15%. In all other cases, the crystals could be frozen after the concentration

of pentaerythritol ethoxylate (15/4 EO/OH) had been increased to 30% in a similar manner.

All data sets for the ferrochelatase crystals were collected at The Advanced Photon Source and SER-CAT on beamline 22-ID. Phases were obtained by using a single monomer of ferrochelatase, taken from the model of the wild-type enzyme [Protein Data Bank (PDB) entry 2QD4], as a molecular replacement search model. Molecular replacement was performed using CNS,<sup>31</sup> version 1.2. Initially, the [2Fe-2S] cluster was omitted from the molecular replacement search model so that strong positive peaks in the difference map could be used as indicators of reasonable solutions based on the positions of the iron atoms. Once reasonable solutions had been identified for the entire asymmetric unit, CNS was also used to perform rigid body refinement and to generate a composite omit map using the simulated annealing protocol. Iterative rounds of model building and refinement were performed with COOT<sup>32</sup> and CNS, respectively. Typically, the backbone and [2Fe-2S] cluster were initially modeled on the basis of the composite omit map and difference maps, and then the side chain atoms, complete with any potential alternate conformations, were modeled before water molecules were placed. Data collection and refinement statistics for all structures are listed in Table 1. Coordinates for all structures have been deposited in the PDB, and PDB entries are listed in Table 1. All graphical representations were created using PyMol,<sup>33</sup> WinCoot,<sup>34</sup> and Caver.<sup>35</sup>

**Table 1. Data Collection and Refinement Statistics for Variants of Human Ferrochelatase Presented Here**

	H240A	F337R	F110A/S197C
resolution range (Å) <sup>a</sup>	50.0–1.8 (1.86)	50.0–1.8 (1.86)	50.0–2.5 (2.59)
$R_{\text{sym}}$ (%) <sup>b</sup>	8.2 (28.1) <sup>c</sup>	8.9 (32.7)	8.7 (22.7)
$I/\sigma$	38 (4)	40 (5)	11 (2)
redundancy	8 (5)	9 (6)	5 (3)
no. of unique reflections	163439	165727	30208
$R_{\text{cryst}}$ (%)	18.5	17.5	22.3
$R_{\text{free}}$ (%)	22.3	21.7	28.0
rmsd for bonds (Å)	0.007	0.008	0.008
rmsd for angles (deg)	1.3	1.34	1.4
average <i>B</i> factor	18.0	19.2	40.8
PDB entry	3AQI	4F4D	4F4G

<sup>a</sup>Numbers in parentheses represent the lower-resolution limit for the outer resolution shell. <sup>b</sup> $R_{\text{sym}} = \sum_{hkl} [\sum_i (|I_{hkl,i}| - \langle I_{hkl} \rangle)] / \sum_{hkl,i} |I_{hkl,i}|$ , where  $I_{hkl}$  is the intensity of an individual measurement of the reflection with indices *hkl* and  $\langle I_{hkl} \rangle$  is the mean intensity of that reflection. <sup>c</sup>Numbers in parentheses represent the value for the outer resolution shell.

## RESULTS AND DISCUSSION

Ferrochelatase is associated with the matrix side of the mitochondrial inner membrane.<sup>6</sup> Because the active site pocket of ferrochelatase opens into the mitochondrial inner membrane but does not span the membrane, the acquisition of substrates requires the transmembrane transport of both iron and porphyrin. Biochemical data support a model whereby ferrochelatase acquires protoporphyrin directly across the membrane from the previous enzyme, protoporphyrinogen oxidase, via a transient complex.<sup>36,37</sup> In addition, with the availability of crystallographic structures for both ferrochelatase



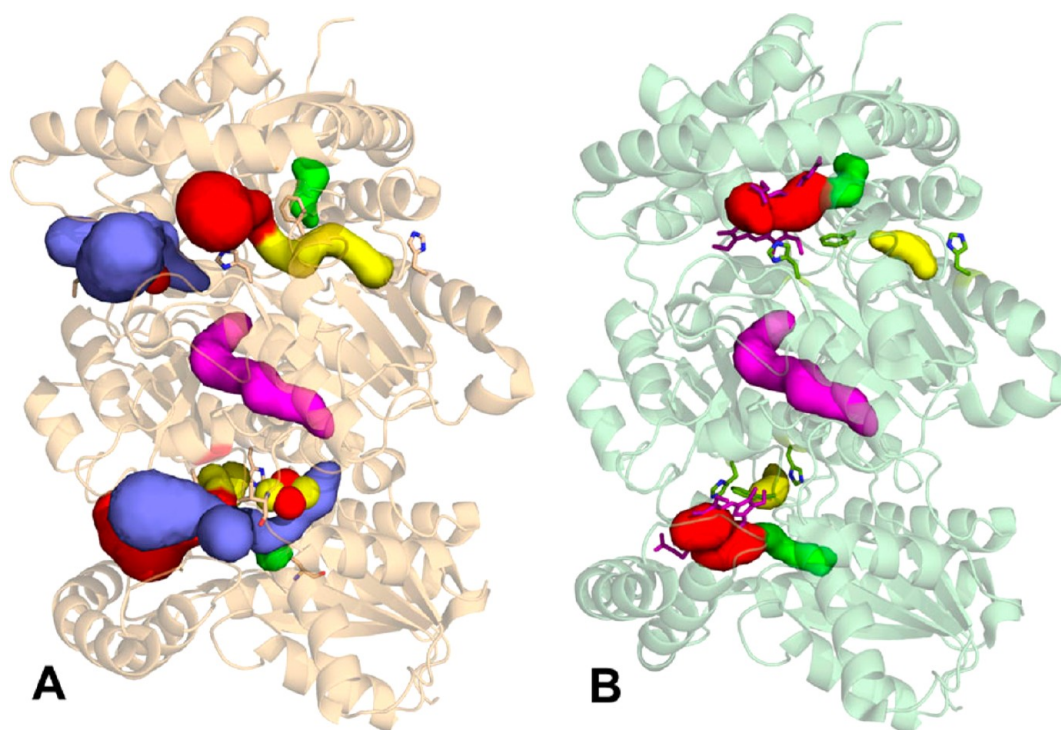


**Figure 2.** Human ferrochelatase channels. (A) All channels present in the open conformation (PDB entry 2HRC). The channels are colored as follows: H240 in yellow, Q139 in green, cluster in blue, and dimer interface in magenta. The active site pocket is highlighted in red and is continuous with the H240 channel in the open conformation. (B) H240, Q139, and dimer interface channels in the closed conformation (PDB entry 2QD1). The bound protoporphyrin IX is shown as purple sticks, and the active site pocket is highlighted in red. The Q139 channel is continuous with the active site in the closed conformation. The side chains of residues H240, H263, and F337 are shown as sticks in each panel.

and protoporphyrinogen oxidase, in silico docking exercises demonstrate that such an interaction can occur<sup>38</sup> (Figure S2 of the Supporting Information). No evidence supports the transit of iron via the same route as porphyrin from protoporphyrinogen oxidase, and thus another pathway likely exists for ferrochelatase to obtain ferrous iron. The acquisition of substrate iron could occur from a transmembrane transporter via the main opening to the active site pocket of ferrochelatase only if considerable molecular motion, or rocking, of ferrochelatase occurs within the membrane.

Recent data provide support for a model of iron acquisition from the inner mitochondrial membrane iron transporter mitoferrin 1.<sup>19</sup> Mitoferrin 1 is a typical mitochondrial inner membrane solute transporter that spans the membrane, so transported iron will be available on the matrix side of the inner mitochondrial membrane<sup>39</sup> (Figure S3 of the Supporting Information). Hunter and Ferreira<sup>23</sup> have proposed that ferrochelatase may obtain iron from mitoferrin or frataxin via the extended  $\pi$ -helix of the enzyme. Iron would then follow a track composed of the conserved acidic residues along the  $\pi$ -helix. This suggestion has also been made by others for the *B. subtilis* ferrochelatase in which the helix has not been observed to extend.<sup>40</sup> This role of the  $\pi$ -helix is not supported by amide hydrogen–deuterium exchange experiments conducted with human ferrochelatase.<sup>41</sup> Two substantial discrepancies between the Hunter and Ferreira model and published data currently exist.<sup>23</sup> First, their model is based upon a single monomer, not the homodimer, and spatially misrepresents published data with regard to the overall orientation of the native homodimeric protein relative to the membrane.<sup>42,43</sup> The region they cite as the membrane binding surface is, in fact, the dimer interface. Thus, their homodimer would be oriented with one subunit

completely submerged in the lipid bilayer and the other completely exposed within the matrix space. All available crystal structures of dimeric human ferrochelatase are consistent with a spatial orientation in which the  $\pi$ -helix unwinds into the membrane and not back up into the matrix (Figure S4 of the Supporting Information). Second, no data show that metal ions bind to residues of the  $\pi$ -helix when it is in the unwound state. Indeed, available data suggest that the helix extension is related to heme release, and in the absence of heme, there is nothing to stabilize the extended helix. Thus, the model proposed by Hunter and Ferreira<sup>23</sup> would require the simultaneous exit of heme and the entrance of iron via the same path. In the absence of product release, no substrate iron would bind, which does not fit with the overall kinetic analysis<sup>16,44–46</sup> or structural studies.<sup>11–13,22,40,43,47</sup> We believe that a more reasonable hypothesis is that iron is donated from mitoferrin (or possibly via an as yet unidentified iron chaperone intermediate) directly to a matrix-exposed iron portal on the surface of ferrochelatase and then transits to the active site via a solvent-filled channel.

**Solvent-Filled Channels.** Examination of the available crystal structures of wild-type and variants of human ferrochelatase (Table S1 of the Supporting Information) reveals the presence of four solvent-filled channels within the protein (Figure 2) that are of sufficient size to accommodate water and/or a desolvated metal ion. In the determined structures, these channels contain well-ordered water molecules that show some conservation between species. In this discussion, two channels are named on the basis of the terminal residue of the channel within the human enzyme (i.e., H240 and Q139). Two additional channels are named for the structures with which they are associated (i.e., cluster channel and dimer interface channel).

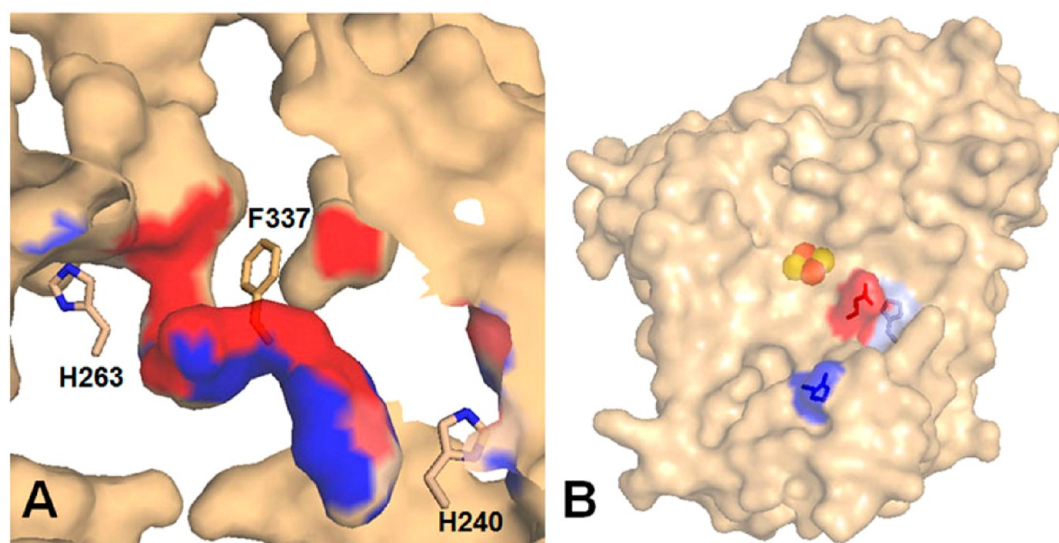


**Figure 3.** Channel and surface views of the H240 channel. Panel A shows the amphipathic nature of the H240 channel. Hydrophobic residues that contribute to the surface of this channel are colored blue and polar residues red. The catalytic histidine, H263, and residues F337 and H240 are shown as sticks and labeled. Panel B shows the surface representation of the matrix-exposed face of the open conformation (PDB entry 2HRC) with residues H240 (light blue), R366 (dark blue), and E369 (red) shown as sticks.

Channel H240 is found in the human and *S. cerevisiae* ferrochelatase structures. It is open to the back of the active site pocket when the enzyme is in the open conformation (Figure 2A). Channel Q139 is a shorter channel that is present in the *B. subtilis*, human, and *S. cerevisiae* structures. However, in the human enzyme, it is open to the active site pocket only with bound porphyrin (closed conformation) (Figure 2B). The cluster channel is a tunnel found in the human enzyme that originates at the protein surface near the opening, or lip, of the active site pocket (at V407) and continues past the [2Fe-2S] cluster. The lip region of the enzyme is proposed to be the portion of the protein that is associated with the inner mitochondrial membrane.<sup>43</sup> The cluster channel is absent in *B. subtilis* and *S. cerevisiae* ferrochelatases, which both lack a [2Fe-2S] cluster. Also lacking in the monomeric *B. subtilis*, but present in both human and *S. cerevisiae* ferrochelatase, is an internal channel starting at R298 that spans the dimer interface.

**Channel H240.** This channel extends from H240 on the matrix-exposed or “back” side of the protein into the active site pocket. The imidazole of H240 forms a flap covering the channel end, but there is no obstruction to this side chain being able to flip aside, thus opening a direct, although tortuous, solvent-filled pathway to the active site pocket. In the substrate free form of the enzyme, this channel is open to the active site (Figure 2A). However, the channel is gated at the distal end from H240 during the catalytic cycle by the side chain of F337. The tunnel is amphipathic in nature, with one side being polar and the other being hydrophobic (Figure 3A). The side chains and backbone atoms of the following residues make up the surface of the H240 channel: F237, H240, I241, Q302, V333, P334, A336, F337, S339, H341, E343, T344, L348, A368, S370, and L371. Located on the surface of the enzyme adjacent to the opening of the H240 channel are residues R366 and E369 (Figure 3B), whose side chains are surface-exposed for possible protein interactions.

The H240 channel in the open conformation is sufficiently large to allow for egress of active site water as the porphyrin macrocycle enters the active site and/or the entrance of the desolvated ferrous iron substrate. Upon porphyrin binding, the

benzyl side chain of F337 moves into a position to close the H240 channel that concomitantly opens channel Q139 to the active site. Following metal insertion and as part of the product release mechanism, the side chain of F337 swings back to reopen channel H240. This may facilitate the re-entry of water into the active site as the heme product departs. The possibility that the Q139 channel could be a site in which substrate iron is sequestered to be available only when F337 swings to open the channel upon porphyrin binding exists but seems unlikely because no structure of ferrochelatase in any conformation has been obtained with a bound iron atom in this channel.

To examine the possibility that the H240 channel serves as an iron portal that obtains substrate iron from a donating partner protein in situ, we conducted two sets of experiments. In the first, we examined the impact of mutations of surface residues R366 and E369, which surround the H240 channel opening on the back side of ferrochelatase (Figure 3B), in vivo by assessing the growth and heme production of cells with these variants. In the second, the impact of altering the side chains of channel-lining residues on enzyme activity was determined in vitro.

The in vivo experimental model employed the ferrochelatase deficient *S. cerevisiae* mutant  $\Delta$ hem15.<sup>29</sup> R366 and E369 are conserved between human and *S. cerevisiae* ferrochelatases, although there is a conservative replacement of the histidine at position 240 in the human form with glutamine (N212) in the yeast. A low-copy number plasmid encoding the *S. cerevisiae* ferrochelatase promoter-regulated wild-type human ferrochelatase complements the  $\Delta$ hem15 yeast mutant as well as the plasmid-encoded *S. cerevisiae* ferrochelatase (Table S2 of the Supporting Information). This complementation is of note because the human enzyme differs from the *S. cerevisiae* ferrochelatase in that it possesses a [2Fe-2S] cluster that is essential for activity.<sup>48</sup> A number of variant human ferrochelatases were analyzed for their ability to support growth and heme synthesis of  $\Delta$ hem15 yeast. Among the enzyme variants examined were some that have previously been shown to have little or no measurable enzyme activity in vitro (H263C and R164L/Y165L),<sup>25</sup> thus, these served as negative



controls. As expected, these variants did not support normal growth or heme production of the  $\Delta hem15$  yeast mutant (Table 2).

**Table 2. In Vivo Analysis of Human Ferrochelatase Surface and Active Site Variants<sup>a</sup>**

variant	complementation of $\Delta hem15$	heme synthesis (% of wild-type value)
Y165F	yes	56
H263C	no	—
R164L/Y165L	no	—
H240A	yes	89
H240E	yes	56
E369T	yes	86
H240A/R366E	yes	53
H240A/E369T	yes	36
H231A/D383A	yes	71
H231A/D383K	yes	84
R290E	yes	92
E289K	yes	100
E289A/R290A	yes	85

<sup>a</sup>Heme synthesis values represent the average of the heme content from three different experiments with a <10% standard deviation.

The H240 channel openings are on either side of the homodimeric ferrochelatase as it is proposed to sit on the membrane, thus placing them in a position that is spatially close to where one might expect an adjacent mitoferrin molecule to be (Figure 4A,B and Figure S3 of the Supporting Information). To investigate the possibility that the H240 channel has a role in substrate iron acquisition, we created variants in which the imidazole side chain of H240 was replaced with either a smaller, uncharged alanine (H240A) or an acidic side chain (H240E). Interestingly, the H240A variant-expressing  $\Delta hem15$  had close to normal heme synthesis, while the H240E variant had significantly reduced cellular heme levels (Table 2). Because R336 and E369 are residues located on the surface in the proximity of H240 and might be involved in complementary charge pair interactions with an interacting, iron supply protein, we created the H240A/R366E and H240A/E369T variants. When these H240A/R366E and H240A/E369T double variants were expressed in  $\Delta hem15$ , reduced amounts of

heme were synthesized. These data are consistent with the hypothesis that the matrix surface of the H240 channel is involved in obtaining iron from a donor protein.

To ensure that the H240A mutation did not have an impact on the overall structure and/or orientation of active site residues, the H240A variant was crystallized and its structure determined to 1.8 Å. This variant revealed a structure very similar to the open conformation of the wild-type enzyme and R115L variant with a root-mean-square deviation (rmsd) between C $\alpha$  atoms of 0.358 Å, as well as a similar orientation of most amino acid side chains. One difference observed in the H240A structure is the presence of a Mg<sup>2+</sup> atom coordinated via water molecules to several residues of the conserved  $\pi$ -helix (E347, Y352, and E351) and the backbone atoms of K304 (Figure S1 of the Supporting Information).

In addition, a selection of surface variants on the back side of the enzyme distant from H240 that have previously been reported to bind cobalt (H231A/D383A and H231A/D383K)<sup>43</sup> (Figure 4A,B) were examined. Assuming that the charged surface residues at the cobalt-binding site were essential for metal binding and that by eliminating these charges the affinity of the enzyme for substrate metal would be significantly diminished, we created variants in which the charges of the putative metal-binding residues were eliminated (H231A/D383A) or altered by changing the acidic glutamate to a basic lysine (H231A/D383K). None of these alterations had any significant impact on the ability of  $\Delta hem15$  cells to produce heme, suggesting that the previously identified cobalt-binding site<sup>43</sup> is not necessary for normal iron delivery.

It has also been proposed by some that the small mitochondrial matrix iron-binding protein frataxin is responsible for the delivery of iron to ferrochelatase.<sup>50</sup> Surface residues R290 and E289 have been suggested to provide a putative docking site on ferrochelatase for the delivery of iron from frataxin. Thus, we individually changed the charge of both residues (R290E and E289K) and collectively eliminated the side chain charge of both residues (E289A/R290A), assuming that such alterations would diminish or abolish the affinity of ferrochelatase for frataxin. None of these variants resulted in a significant phenotype in the complemented  $\Delta hem15$  yeast cells (Table 2). This suggests that if frataxin serves as an iron donor, it is not via this site.

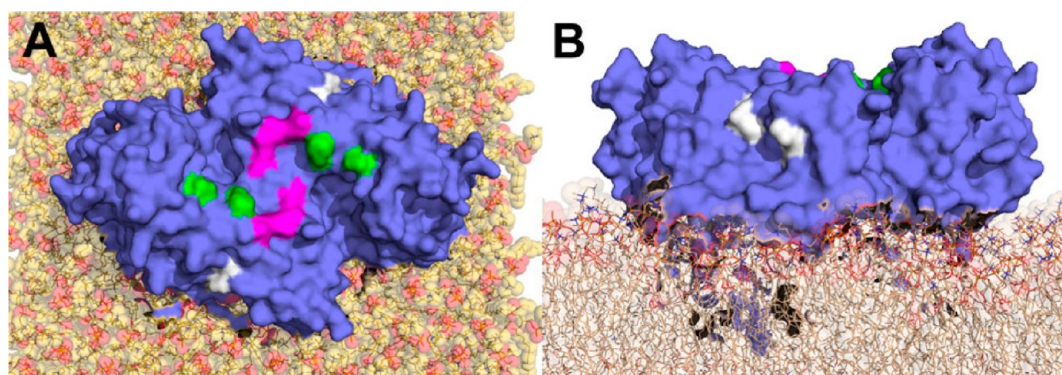


**Figure 4.** Location of surface residues on human ferrochelatase. Human ferrochelatase (PDB entry 2HRC) shown as a slate surface representation is modeled into a lipid bilayer (tan or yellow sticks) (PDB DLPC\_303K<sup>49</sup>). Surface patches representing the surface of the H240A channel (R366 and E369), cobalt-binding residues (H231 and D383), and putative frataxin docking residues (E289 and R290) are colored white, magenta, and green, respectively. Panel A shows the enzyme surface from the matrix side of the inner mitochondrial membrane, and panel B shows a side profile of the enzyme embedded in the membrane.

If the H240 channel is an iron portal, one would expect that alteration of the residues lining the tunnel would have an impact on enzyme activity. Thus, a number of H240 channel variants were purified and characterized. For these variants, the ability to complement the ferrochelatase-lacking *E. coli*  $\Delta hemH$  and kinetic parameters for the purified enzyme were examined (Table 3). For two variants, individual polar side chains

**Table 3. Kinetic Parameters for Wild-Type and Variant Human Ferrochelatases<sup>a</sup>**

	$K_m$ iron ( $\mu M$ )	$K_m$ meso ( $\mu M$ )	$k_{cat}$ ( $min^{-1}$ )	rescue $\Delta hemH$
wild type <sup>13</sup>	18	28	4.2	yes
R115L <sup>13</sup>	21	34	3.2	yes
N75A <sup>20</sup>	33.8	16.8	0.96	yes
I132A	ND <sup>b</sup>	ND <sup>b</sup>	ND <sup>b</sup>	yes
Q139A	ND <sup>b</sup>	ND <sup>b</sup>	ND <sup>b</sup>	yes
Q139L	26.2	26.7	0.60	yes
S201A	8.4	13.2	1.8	yes
F237Y	13.8	ND <sup>b</sup>	0.8	yes
F237L	16	14	1.4	yes
H240A	27.6	12.1	3.42	yes
H240E	21.1	12.6	2.8	yes
H240K	27.9	17.9	4	yes
I241F	21.5	11.3	1	yes
Q302A	52.6	29.3	4.5	yes
Q302D	c	c	c	yes
V333A	ND <sup>b</sup>	ND <sup>b</sup>	ND <sup>b</sup>	yes
V333S	ND <sup>b</sup>	ND <sup>b</sup>	ND <sup>b</sup>	yes
P334L	48.8	18.2	0.56	yes
F337A <sup>20</sup>	17.8	24.6	0.81	yes
F337R	c	c	c	no
S339A	ND <sup>b</sup>	ND <sup>b</sup>	ND <sup>b</sup>	yes
T344A	25.9	20.1	0.65	yes
T344K	c	c	c	no
A368C	16.8	51.9	3.28	yes
A368F	c	c	c	yes
A368L	18.1	36.9	0.94	yes
S370A	39.7	11.4	3.1	yes
S370C	40	33	3	yes

<sup>a</sup>Values reported represent the average parameters determined from four separate experiments with a <10% standard deviation. <sup>b</sup>Not determined. <sup>c</sup>Not measurable.

contributing to the surface of the channel were replaced with alanine (Q302A and S370A). In one instance, the polar uncharged side chain of residue S370 was replaced with cysteine, a potentially strong iron ligand. All three variants (Q302A, S370A, and S370C) exhibited an increased  $K_m$  for iron. Variants F237Y and A368L, which introduced modest alterations in side chain polarity or size, showed decreases in  $k_{cat}$ . A similar result was found for the P334L variant. Two more drastic variants, F337R and T344K, lacked measurable enzyme activity and did not complement the *E. coli*  $\Delta hemH$  mutant. Interestingly, T344 is also a component of the conserved  $\pi$ -helix and is located close to residue H341 (below). The change in size and charge that occurs in the T344K variant may allow it to interact with H341, resulting in the reorientation of H341 and thus loss of activity.

Unfortunately, the indisputable designation of the H240 channel as a conduit for substrate iron based upon in vitro assays is problematic. Even if the H240 channel is the natural

iron portal, it is reasonable to assume that variants with a partial or completely blocked channel may still have some measurable in vitro activity that would be attributable to iron diffusing into the mouth of the active site in the enzyme assay. Given that channel variants have no impact on overall enzyme structure and, with the exception of F337, are not located within the active site pocket, any enzyme activity diminution would be expected to result from an inability of the channel to provide its normal function. Variants completely lacking activity could thus represent enzymes in which the mutation disrupts the normal catalytic cycle. As discussed below, we posit that this is what occurs in the F337R variant.

**Channel Q139.** A shorter channel that is present in all published ferrochelatase structures is the Q139 channel. In the wild-type human enzyme, the Q139 channel is open to the active site only in the closed (substrate-bound) conformation.<sup>8,13</sup> However, in structures in which the active site hydrogen bonding network has been disrupted, such as has been reported to occur for the variants possessing the H263C or H341C mutation, and in the F337A variant where the physical barrier attributable to the F337 side chain is missing, the Q139 channel is open to the active site pocket.<sup>20</sup> N75, I132, T136, Q139, F163, Q190, F337, and T338 are found to line channel Q139.

To investigate potential roles that residues lining the Q139 channel may play, enzyme variants possessing I132A and Q139A/L were constructed and their activity was assessed by rescue of *E. coli*  $\Delta hemH$  (Table 3). All of these variants possessed enzyme activity sufficient to rescue the  $\Delta hemH$  mutant. To further investigate the Q139L variant, in vitro assays were performed (Table 3). This variant possessed a significantly diminished  $k_{cat}$ . The F337A and N75A variants of human ferrochelatase, which were produced and analyzed in previous studies, also possess decreased  $k_{cat}$  values.<sup>20</sup> The diminished enzyme activity of F337A is of note because its structure is very similar to that of the wild-type enzyme with an intact open conformation hydrogen bond network. The only substantial difference between the wild-type enzyme and F337A variant is that both the H240 and Q139 channels are simultaneously open to the active site in the variant. N75 is of interest because previous and current studies suggest that it bridges the hydrogen bond networks found in the upper and lower active site pocket (see below and ref 20).

It is of note that an equivalent to the human Q139 channel is observed in the *B. subtilis* ferrochelatase structures. This channel is continuous with the active site pocket and also open at the protein surface in most structures.<sup>9,10,22,40,47,51,52</sup> Analysis of the alanine variants of the equivalent of Q139 (residue Q63 in *B. subtilis*) showed decreased in vitro activity yet unchanged in vivo activity as assessed by growth measurements.<sup>53</sup> From the results presented herein as well as the *B. subtilis* studies, the role of the Q139 channel in the catalytic mechanism is unclear.

**Cluster Channel.** The cluster channel originates at the active site lip region at residue V407, passes by the [2Fe-2S] cluster, and ends just short of the dimer interface channel at residue R298 (Figure 5). Interestingly, it is the guanidino side chain of R298 from the B subunit that intercalates into the A subunit thereby blocking the A subunit cluster channel from the dimer interface channel (below) and vice versa. The cluster channel and its opening are lined by residues D95, D97, L98, Y194, C196, S197, G199, S201, L203, N204, R226, R272, Q398, L399, S402, C403, C406, V407, N408, C411, T414, and K415.



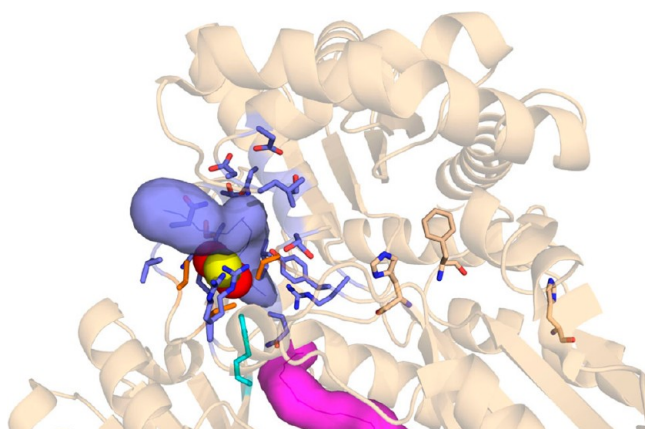


**Figure 5.** Cluster channel. The cluster channel is shown in slate. Residues that contribute to the surface of the cluster channel are shown as sticks. For reference, the dimer interface channel is colored magenta, active site residues H263 and F337 are shown as wheat sticks, residue R298 from the B subunit is colored cyan, and the four cysteine residues that serve as ligands for the [2Fe-2S] cluster are shown as orange sticks.

Four of these residues (C196, C403, C406, and C411) are the coordinating residues for the [2Fe-2S] cluster that forms a portion of one wall of the channel.

Only one residue in the cluster channel was investigated, and the kinetic parameters for the S201A (inside the channel across from the cluster) variants are listed in Table 3. This variant possessed diminished  $K_m$ s and  $k_{cat}$  values. Given that this residue also has access to the active site pocket, it may play a role in the hydrogen bonding network.

The structure of the F110A/S197C variant was determined to 2.6 Å. The structure of this variant is very similar to the open conformation with minimal differences in the orientation of side chain residues for most amino acids (rmsd for C $\alpha$  atoms of 0.448 Å). This double variant rescued *E. coli*  $\Delta hemH$ , although kinetic parameters were not determined. Given its position and the fact that the *S. cerevisiae* ferrochelatase lacks a [2Fe-2S] cluster, it would appear unlikely that the cluster channel is directly involved in iron acquisition. However, for ferrochelatases that possess the cluster, this channel, which provides an aqueous channel to the cluster, may play some role in the catalysis or regulation of activity.

**Dimer Interface Channel.** The dimer interface channel is formed between the interface of the two ferrochelatase monomers (A and B). Interestingly, the channel structure is conserved between the human and *S. cerevisiae* ferrochelatases despite the significant lack of homology of residues between these two proteins at the dimer interface. The channel is lined by identical residue participants from both subunits, including V270, D274, P275, P277, Q278, E279, S281, Y297, R298, L299, W301, L311, G312, P313, and Q398 (Figure 6). Thus, it possesses 2-fold symmetry with regard to charge distribution. In the crystal structures, this channel is closed at both ends. The channel is separated from the end of the cluster channel (A subunit) by the side chains of R298 (of the B subunit) and Q398 (of the A subunit). Access from the channel to the enzyme surface is blocked by only the hydroxyl group of Y297 (of the B subunit) and the carboxyl group of E279 (of the A subunit). One could imagine that with minimal molecular movement the channel could open to the protein surface and/or the cluster channels. Thus, it is not surprising that in some

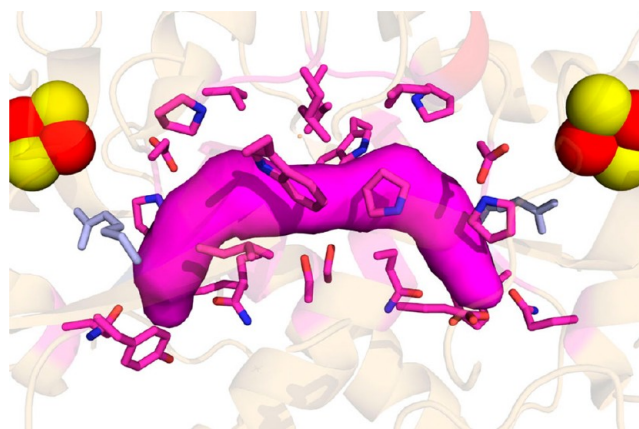


**Figure 6.** Dimer interface channel. The channel found at the dimer interface is colored magenta. Residues from each subunit that contribute to the surface of this channel are shown as sticks, and the [2Fe-2S] clusters from each subunit are shown as red and yellow spheres. The side chain of residue R298 from each subunit is shown as light blue sticks.

structures one finds a glycerol molecule in this channel,<sup>12</sup> indicating that sufficient molecular mobility exists to allow access of small molecules present in the crystallization solvent to this interior channel. Because this channel does not have access to the active site, a role for this channel in substrate delivery is not readily apparent.

**Channel Gating by F337 and Its Relationship to the Catalytic Cycle.** F337 is a conserved residue located at the back side of the active site pocket. Structural data from human ferrochelatase demonstrate that the orientation of the benzyl ring of F337 determines whether the H240 or Q139 channels are open to the active site pocket. It is of note that F337 is part of a loop that connects  $\beta$ -strand 7 and the  $\pi$ -helix. Thus, rotation of F337 has the potential to influence and/or be influenced by the secondary structure of this region.

In an effort to understand what may control the movement of F337 and determine if it serves solely as a gatekeeper or has additional functions during catalysis, the structure and function of two ferrochelatase variants were investigated. In one, the benzyl side chain was replaced with the spatially smaller methyl group of alanine (F337A), and in another, it was replaced with a bulky, charged guanidino group of arginine (F337R). The previously described F337A variant does not have any alterations in the resting state hydrogen bond network in the active site but exhibits a 5-fold reduction in  $k_{cat}$ .<sup>20</sup> Thus, the benzyl group and/or the ability to gate the H240 and Q139 channels is not essential for enzyme activity, but in its absence, the activity of ferrochelatase is significantly impaired.

The F337R variant was constructed, expressed, and characterized. The F337R variant has no detectable catalytic activity and is not purified or crystallized with a bound substrate or product as is typical of wild-type human ferrochelatase. The structure of this variant was determined to 1.8 Å. This variant possesses an open conformation with cholate molecules present in each active site as well as in the entry route to the active site as is observed for the wild-type human ferrochelatase in the open conformation. However, in the F337R variant enzyme, one of the active site cholate molecules is rotated 180° compared to its position in the active site of the open conformation wild-type (PDB entry 2QD3<sup>13</sup>) and R115L variant ferrochelatases (PDB entry 2HRC<sup>8</sup>). This would



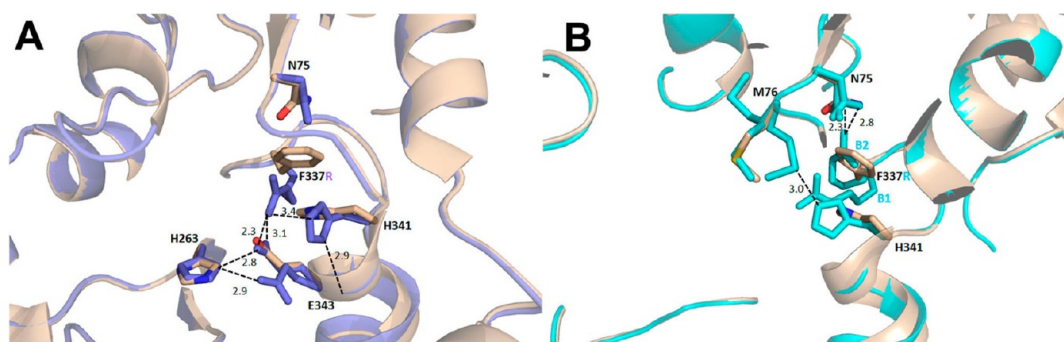


**Figure 7.** Comparison of the active site of the inactive variant F337R and wild-type ferrochelatase. (A) Orientation of F337R in the A monomer and the B1 conformers in the B monomer and its interactions with residues in the bottom of the active site pocket of ferrochelatase. Hydrogen bonding interactions in the F337 variant are indicated with dashed lines and distances in angstroms. Wild-type active site residues are colored wheat, blue, red, and yellow for carbon, nitrogen, oxygen, and sulfur atoms, respectively. Active site residues of the F337R variant are shown in slate. (B) Orientations of F337R in the active site of the B monomer. Hydrogen bonding interactions of the B2 conformer of F337R with N75 in the top of the active site are indicated as described in panel A. The distance between H341 and one conformer of M76 in the F337R variant is also shown. Wild-type residues are shown as described in panel A, and those of the B monomer of F337R are colored cyan.

indicate that the overall surface potential within the active site of the F337R variant is altered from that found in the wild-type protein, which could alter substrate binding. Also of note is the likelihood that the H240 and/or Q139 channel is blocked at their entrance to the active site by the F337R side chain, thereby preventing iron entry and/or water movement through the channel.

Upon examination of the two subunits (“A” and “B”) of the homodimeric F337R variant human ferrochelatase, the orientations of the guanidino side chains of residue 337 differ between the A and B subunits. In the A monomer, the side chain of R337 is best modeled in a single orientation with 100% occupancy. However, in the B monomer, the guanidino group is best modeled in two orientations, each with 50% occupancy (e.g., B1 and B2) (Figure 7). One of these two orientations (B1) is identical to what is observed in the A monomer at all times. In this orientation, the A and B1 R337 guanidino group is within hydrogen bonding distance of the side chains of residues H263, H341, and E343 (Figure 7A). H341 and E343 comprise part of the catalytically important  $\pi$ -helix. Hydrogen bonding between the R337 guanidino group in this conformation and the imidazole of H341 explains the observed 90° rotation of H341 away from what is seen in the wild-type enzyme (Figure 7A). In this orientation, H341 can no longer participate in the hydrogen bonding network found in the wild-type open conformation but instead forms a hydrogen bond with a backbone amine group of the amino terminus of the  $\pi$ -helix. In structural models of the B2 monomer, the guanidino side chain is within hydrogen bonding distance of N75 at the top of the active site pocket (Figure 7B). As a result, the position and orientation of N75 are distinctly different from those found in both subunits of the wild-type enzyme, and in the A subunit model of the F337R variant. In addition, and only in the B monomer, residue M76, also at the top of the active site pocket opposite H263, is found in three distinct conformations. In one of the M76 side chain conformations (50% occupancy), the side chain is closer to the imidazole side chain of H341 than it is in the wild-type enzyme structure.

The changes in active site pocket residue side chain conformations and the hydrogen bond network observed in the structure of the F337R variant may provide some insight into the catalytic cycle. If one considers a model in which iron transits past F337 in its route to chelation, replacement of the

benzyl side chain with the positively charged guanidino side chain in the F337R variant may mimic the presence of the ferrous iron dication at this position. Thus, the altered conformations seen in the variant may represent a snapshot of an intermediate stage of the catalytic cycle. The observation of multiple spatial conformations within the active site of the F337R variant would be consistent with the transient interactions of the iron atom as it moves into position for chelation. Additionally, the spatial reorientation of H341 (above) that includes new hydrogen bonds with backbone atoms of the  $\pi$ -helix will affect several steps in catalysis, including proton abstraction and product release.

Overall, the available data support a role for F337 that is more than that of a simple gatekeeper to the H240 and Q139 channels. The F337R variant structure, in which the hydrogen bond network in the top of the active site is altered depending on the conformation of residue F337R and in the bottom of the active site pocket is partially disrupted by the altered conformation of H341, suggests that this residue may help coordinate structural changes between the top and bottom of the active site and modulate the stability of the  $\pi$ -helix during the catalytic cycle.

## CONCLUSIONS

The means by which iron is transported to residues in the active site of human ferrochelatase and the precise residues involved in active site iron binding remain unanswered questions. At present, the only universal point of agreement appears to be that *in vivo* ferrous iron and protoporphyrin IX will be delivered directly to ferrochelatase, as both of these substrates are potentially toxic to the cell. For higher organisms containing a ferrochelatase whose active site faces the inner mitochondrial membrane, the mechanism of substrate delivery as well as the release of heme becomes substantially more complex. A reasonable solution to delivering protoporphyrin IX can be found in the proposed transient protein–protein complex formed between protoporphyrinogen oxidase and ferrochelatase,<sup>36–38</sup> but the delivery of the ferrous iron must involve additional steps that include desolvation of the hydrated ion. One possible mechanism that has not been explored is the role of enzyme channels in desolvating and delivering the metal ion from carriers to the active site. Specifically, the existence of several water-filled channels that originate in the active site and

end at the protein surface could provide a sheltered conduit by which the redox active ferrous iron substrate could enter from the matrix side of the mitochondrial membrane and move to the active site without being exposed to the bulk medium. Such access would allow donation of iron either directly from a membrane-spanning transporter (mitoferrin<sup>19</sup>) or from a matrix protein without exposing the reactive ferrous iron to the matrix environment. Movement of substrate iron into the active site in this way could provide a means by which the entry of metal into the active site is regulated to control the ordered reaction catalyzed by ferrochelatase.

Data provided herein support the role of the H240 channel in iron delivery. In addition, the channel could also serve as an aqueduct for entry and exit of water molecules from the active site to facilitate substrate binding of both protoporphyrin and iron, and product release. These types of aqueducts have been observed in cytochrome P450 enzymes and are thought to contribute to substrate binding and water-mediated proton release.<sup>54,55</sup> Evidence of the cluster channel as an aqueduct is supported by hydrogen–deuterium exchange studies in the presence of iron.<sup>41</sup> It is possible and likely that the ferrochelatase channels could serve multiple roles and would likely contribute to the regulation of the catalytic mechanism.

Residue F337, which lies at the convergence of the Q139 and H240 channels in the active site, is one of the few conserved residues in all ferrochelatases. Both kinetic and structural studies (this study and ref 20) have suggested that this residue serves as a channel gate and plays a role in regulating the overall reaction mechanisms. We propose the following model for the role of F337. In the open conformation with the resting hydrogen bond network intact, F337 sits above H341, which serves as a cap to the functionally important  $\pi$ -helix. When the porphyrin substrate binds and the closed conformation forms, F337 reorients and leads to the partial disruption of the resting state hydrogen bond network and the initial destabilization of the  $\pi$ -helix. The movement of F337 during the catalytic cycle would likely result in changes in the active site electrostatics and thus be the impetus for the observed movement of the 6-propionate during the catalytic cycle. While heme propionates have been shown in hemoproteins to be important in binding, orienting, and modulating electronic properties,<sup>56</sup> ferrochelatase may use changes in the electronic properties of its active site to influence the orientation of the heme propionates and facilitate product release. Following chelation and proton abstraction by H263 and E343, the concomitant disruption of the hydrogen bond network destabilizes the  $\pi$ -helix, allowing for it to unwind for product release. These proposed roles of F337 are consistent with the data presented herein as well as previous studies.<sup>20</sup>

## ■ ASSOCIATED CONTENT

### ■ Supporting Information

Additional figures, including the Mg<sup>2+</sup> ion in the H240A ferrochelatase structure (Figure S1) and models of ferrochelatase and protoporphyrinogen oxidase (Figure S2), ferrochelatase and mitoferrin (Figure S3), and ferrochelatase in different conformations (Figure S4) in the membrane, and tables summarizing all structures of human ferrochelatase (Table S1) and the validation of  $\Delta$ hem15 rescue (Table S2). This material is available free of charge via the Internet at <http://pubs.acs.org>.

## Accession Codes

Protein Data Bank entries 3AQI, 4F4D, and 4F4G for H240A, F337R, and F110A/S197C, respectively.

## ■ AUTHOR INFORMATION

### Corresponding Author

\*Telephone: (706) 542-7843. E-mail: [medlock@uga.edu](mailto:medlock@uga.edu). Fax: (706) 542-5285.

### Present Addresses

<sup>†</sup>Department of Pharmaceutics and Translational Therapeutics, University of Iowa College of Pharmacy, Iowa City, IA 52242.

<sup>‡</sup>Athens Research & Technology, Athens, GA 30601.

### Funding

This research was supported by National Institutes of Health Grant DK32303 to (H.A.D.) and National Science Foundation Grant MCB0835432 (W.N.L.).

### Notes

The authors declare no competing financial interest.

## ■ ACKNOWLEDGMENTS

We thank Dr. Walter K. Schmidt (University of Georgia) for providing the yeast shuttle vector, Drs. Jerry Kaplan and R. J. Crisp (University of Utah) for providing the  $\Delta$ hem15 and wild-type *S. cerevisiae* strains as well as expert advice on the in vivo experiments, Amy E. Burden for preparation of several human ferrochelatase variants, and Mrs. Michael Carter and Michael Kasson who worked on crystal growth of the F337R variant.

## ■ REFERENCES

- (1) Burris, T. P. (2008) Nuclear hormone receptors for heme: REV-ERB $\alpha$  and REV-ERB $\beta$  are ligand-regulated components of the mammalian clock. *Mol. Endocrinol.* 22, 1509–1520.
- (2) Faller, M., Matsunaga, M., Yin, S., Loo, J. A., and Guo, F. (2007) Heme is involved in microRNA processing. *Nat. Struct. Mol. Biol.* 14, 23–29.
- (3) Mense, S. M., and Zhang, L. (2006) Heme: A versatile signaling molecule controlling the activities of diverse regulators ranging from transcription factors to MAP kinases. *Cell Res.* 16, 681–692.
- (4) Dailey, T. A., Boynton, T. O., Albetel, A. N., Gerdes, S., Johnson, M. K., and Dailey, H. A. (2010) Discovery and characterization of HemQ: An essential heme biosynthetic pathway component. *J. Biol. Chem.* 285, 25978–25986.
- (5) Burden, A. E., Wu, C., Dailey, T. A., Busch, J. L., Dhawan, I. K., Rose, J. P., Wang, B., and Dailey, H. A. (1999) Human ferrochelatase: Crystallization, characterization of the [2Fe-2S] cluster and determination that the enzyme is a homodimer. *Biochim. Biophys. Acta* 1435, 191–197.
- (6) Harbin, B. M., and Dailey, H. A. (1985) Orientation of ferrochelatase in bovine liver mitochondria. *Biochemistry* 24, 366–370.
- (7) Al-Karadaghi, S., Franco, R., Hansson, M., Shelnutt, J. A., Isaya, G., and Ferreira, G. C. (2006) Chelatases: Distort to select? *Trends Biochem. Sci.* 31, 135–142.
- (8) Medlock, A., Swartz, L., Dailey, T. A., Dailey, H. A., and Lanzilotta, W. N. (2007) Substrate interactions with human ferrochelatase. *Proc. Natl. Acad. Sci. U.S.A.* 104, 1789–1793.
- (9) Karlberg, T., Hansson, M. D., Yengo, R. K., Johansson, R., Thorvaldsen, H. O., Ferreira, G. C., Hansson, M., and Al-Karadaghi, S. (2008) Porphyrin binding and distortion and substrate specificity in the ferrochelatase reaction: The role of active site residues. *J. Mol. Biol.* 378, 1074–1083.
- (10) Lecroq, D., Fodje, M., Hansson, A., Hansson, M., and Al-Karadaghi, S. (2000) Structural and mechanistic basis of porphyrin metallation by ferrochelatase. *J. Mol. Biol.* 297, 221–232.

- (11) Karlberg, T., Lecerof, D., Gora, M., Silvegren, G., Labbe-Bois, R., Hansson, M., and Al-Karadaghi, S. (2002) Metal binding to *Saccharomyces cerevisiae* ferrochelatase. *Biochemistry* 41, 13499–13506.
- (12) Medlock, A. E., Carter, M., Dailey, T. A., Dailey, H. A., and Lanzilotta, W. N. (2009) Product release rather than chelation determines metal specificity for ferrochelatase. *J. Mol. Biol.* 393, 308–319.
- (13) Medlock, A. E., Dailey, T. A., Ross, T. A., Dailey, H. A., and Lanzilotta, W. N. (2007) A  $\pi$ -helix switch selective for porphyrin deprotonation and product release in human ferrochelatase. *J. Mol. Biol.* 373, 1006–1016.
- (14) Fodje, M. N., and Al-Karadaghi, S. (2002) Occurrence, conformational features and amino acid propensities for the  $\pi$ -helix. *Protein Eng.* 15, 353–358.
- (15) Dailey, H. A., and Fleming, J. E. (1983) Bovine ferrochelatase. Kinetic analysis of inhibition by N-methylprotoporphyrin, manganese, and heme. *J. Biol. Chem.* 258, 11453–11459.
- (16) Davidson, R. E., Chesters, C. J., and Reid, J. D. (2009) Metal ion selectivity and substrate inhibition in the metal ion chelation catalyzed by human ferrochelatase. *J. Biol. Chem.* 284, 33795–33799.
- (17) Hunter, G. A., Sampson, M. P., and Ferreira, G. C. (2008) Metal ion substrate inhibition of ferrochelatase. *J. Biol. Chem.* 283, 23685–23691.
- (18) Hoggins, M., Dailey, H. A., Hunter, C. N., and Reid, J. D. (2007) Direct measurement of metal ion chelation in the active site of human ferrochelatase. *Biochemistry* 46, 8121–8127.
- (19) Chen, W., Dailey, H. A., and Paw, B. H. (2010) Ferrochelatase forms an oligomeric complex with mitoferrin-1 and Abcb10 for erythroid heme biosynthesis. *Blood* 116, 628–630.
- (20) Dailey, H. A., Wu, C. K., Horanyi, P., Medlock, A. E., Najahi-Missaoui, W., Burden, A. E., Dailey, T. A., and Rose, J. (2007) Altered orientation of active site residues in variants of human ferrochelatase. Evidence for a hydrogen bond network involved in catalysis. *Biochemistry* 46, 7973–7979.
- (21) Hunter, G. A., Al-Karadaghi, S., and Ferreira, G. C. (2011) Ferrochelatase: The Convergence of the Porphyrin Biosynthesis and Iron Transport Pathways. *J. Porphyrins Phthalocyanines* 15, 350–356.
- (22) Hansson, M. D., Karlberg, T., Soderberg, C. A., Rajan, S., Warren, M. J., Al-Karadaghi, S., Rigby, S. E., and Hansson, M. (2011) Bacterial ferrochelatase turns human: Tyr13 determines the apparent metal specificity of *Bacillus subtilis* ferrochelatase. *J. Biol. Inorg. Chem.* 16, 235–242.
- (23) Hunter, G. A., and Ferreira, G. C. (2010) Identification and characterization of an inhibitory metal ion-binding site in ferrochelatase. *J. Biol. Chem.* 285, 41836–41842.
- (24) Mayer, M. R., Dailey, T. A., Baucom, C. M., Supernak, J. L., Grady, M. C., Hawk, H. E., and Dailey, H. A. (2004) Expression of human proteins at the Southeast Collaboratory for Structural Genomics. *J. Struct. Funct. Genomics* 5, 159–165.
- (25) Sellers, V. M., Wu, C. K., Dailey, T. A., and Dailey, H. A. (2001) Human ferrochelatase: Characterization of substrate-iron binding and proton-abstracting residues. *Biochemistry* 40, 9821–9827.
- (26) Frustaci, J. M., and O'Brian, M. R. (1992) Characterization of a *Bradyrhizobium japonicum* ferrochelatase mutant and isolation of the hemH gene. *J. Bacteriol.* 174, 4223–4229.
- (27) Miyamoto, K., Nakahigashi, K., Nishimura, K., and Inokuchi, H. (1991) Isolation and characterization of visible light-sensitive mutants of *Escherichia coli* K12. *J. Mol. Biol.* 219, 393–398.
- (28) Najahi-Missaoui, W., and Dailey, H. A. (2005) Production and characterization of erythropoietic protoporphyrin heterodimeric ferrochelatases. *Blood* 106, 1098–1104.
- (29) Gora, M., Grzybowska, E., Rytka, J., and Labbe-Bois, R. (1996) Probing the active-site residues in *Saccharomyces cerevisiae* ferrochelatase by directed mutagenesis. In vivo and in vitro analyses. *J. Biol. Chem.* 271, 11810–11816.
- (30) Berry, E. A., and Trumpower, B. L. (1987) Simultaneous determination of hemes a, b, and c from pyridine hemochrome spectra. *Anal. Biochem.* 161, 1–15.
- (31) Brunger, A. T. (2007) Version 1.2 of the Crystallography and NMR system. *Nat. Protoc.* 2, 2728–2733.
- (32) Emsley, P., Lohkamp, B., Scott, W. G., and Cowtan, K. (2010) Features and development of Coot. *Acta Crystallogr. D* 66, 486–501.
- (33) *The PyMOL Molecular Graphics System*, version 1.2r3pre, Schrödinger, LLC, New York.
- (34) Emsley, P., and Cowtan, K. (2004) Coot: Model-building tools for molecular graphics. *Acta Crystallogr. D* 60, 2126–2132.
- (35) Chovancová, E., Pavelka, A., Beneš, P., Strnad, O., Brezovský, J., Kozlíková, B., Gora, A., Šustr, V., Klvaňa, M., Medek, P., Biedermannová, L., Sochor, J., and Damborský, J. (2012) CAVER 3.0: A Tool for the Analysis of Transport Pathways in Dynamic Protein Structures (manuscript in preparation).
- (36) Ferreira, G. C., Andrew, T. L., Karr, S. W., and Dailey, H. A. (1988) Organization of the terminal two enzymes of the heme biosynthetic pathway. Orientation of protoporphyrinogen oxidase and evidence for a membrane complex. *J. Biol. Chem.* 263, 3835–3839.
- (37) Proulx, K. L., Woodard, S. I., and Dailey, H. A. (1993) In situ conversion of coproporphyrinogen to heme by murine mitochondria: Terminal steps of the heme biosynthetic pathway. *Protein Sci.* 2, 1092–1098.
- (38) Koch, M., Breithaupt, C., Kiefersauer, R., Freigang, J., Huber, R., and Messerschmidt, A. (2004) Crystal structure of protoporphyrinogen IX oxidase: A key enzyme in haem and chlorophyll biosynthesis. *EMBO J.* 23, 1720–1728.
- (39) Shaw, G. C., Cope, J. J., Li, L., Corson, K., Hersey, C., Ackermann, G. E., Gwynn, B., Lambert, A. J., Wingert, R. A., Traver, D., Trede, N. S., Barut, B. A., Zhou, Y., Minet, E., Donovan, A., Brownlie, A., Balzan, R., Weiss, M. J., Peters, L. L., Kaplan, J., Zon, L. I., and Paw, B. H. (2006) Mitoferrin is essential for erythroid iron assimilation. *Nature* 440, 96–100.
- (40) Hansson, M. D., Karlberg, T., Rahardja, M. A., Al-Karadaghi, S., and Hansson, M. (2007) Amino acid residues His183 and Glu264 in *Bacillus subtilis* ferrochelatase direct and facilitate the insertion of metal ion into protoporphyrin IX. *Biochemistry* 46, 87–94.
- (41) Asuru, A. P., and Busenlehner, L. S. (2011) Analysis of human ferrochelatase iron binding via amide hydrogen/deuterium exchange mass spectrometry. *Int. J. Mass Spectrom.* 302, 76–84.
- (42) Dailey, H. A., and Dailey, T. A. (2003) Ferrochelatase. In *The Porphyrin Handbook* (Kadish, K. M., Smith, K. M., and Guillard, R., Eds.) pp 93–122, Academic Press, San Diego.
- (43) Wu, C. K., Dailey, H. A., Rose, J. P., Burden, A., Sellers, V. M., and Wang, B. C. (2001) The 2.0 Å structure of human ferrochelatase, the terminal enzyme of heme biosynthesis. *Nat. Struct. Biol.* 8, 156–160.
- (44) Dailey, H. A. (1987) Metal inhibition of ferrochelatase. *Ann. N.Y. Acad. Sci.* 514, 81–86.
- (45) Dailey, H. A., Jr., and Lascelles, J. (1974) Ferrochelatase activity in wild-type and mutant strains of *Spirillum itersonii*. Solubilization with chaotropic reagents. *Arch. Biochem. Biophys.* 160, 523–529.
- (46) Gaertner, R. R., and Hollebone, B. R. (1983) The in vitro inhibition of hepatic ferrochelatase by divalent lead and other soft metal ions. *Can. J. Biochem. Cell Biol.* 61, 214–222.
- (47) Lecerof, D., Fodje, M. N., Alvarez Leon, R., Olsson, U., Hansson, A., Sigfridsson, E., Ryde, U., Hansson, M., and Al-Karadaghi, S. (2003) Metal binding to *Bacillus subtilis* ferrochelatase and interaction between metal sites. *J. Biol. Inorg. Chem.* 8, 452–458.
- (48) Dailey, H. A., Finnegan, M. G., and Johnson, M. K. (1994) Human ferrochelatase is an iron-sulfur protein. *Biochemistry* 33, 403–407.
- (49) Domanski, J., Stansfeld, P. J., Sansom, M. S., and Beckstein, O. (2010) Lipidbook: A public repository for force-field parameters used in membrane simulations. *J. Membr. Biol.* 236, 255–258.
- (50) Yoon, T., and Cowan, J. A. (2004) Frataxin-mediated iron delivery to ferrochelatase in the final step of heme biosynthesis. *J. Biol. Chem.* 279, 25943–25946.
- (51) Al-Karadaghi, S., Hansson, M., Nikonov, S., Jonsson, B., and Hederstedt, L. (1997) Crystal structure of ferrochelatase: The terminal enzyme in heme biosynthesis. *Structure* 5, 1501–1510.



(52) Shipovskov, S., Karlberg, T., Fodje, M., Hansson, M. D., Ferreira, G. C., Hansson, M., Reimann, C. T., and Al-Karadaghi, S. (2005) Metallation of the transition-state inhibitor N-methyl mesoporphyrin by ferrochelatase: Implications for the catalytic reaction mechanism. *J. Mol. Biol.* 352, 1081–1090.

(53) Olsson, U., Billberg, A., Sjövall, S., Al-Karadaghi, S., and Hansson, M. (2002) In vivo and in vitro studies of *Bacillus subtilis* ferrochelatase mutants suggest substrate channeling in the heme biosynthesis pathway. *J. Bacteriol.* 184, 4018–4024.

(54) Fishelovitch, D., Shaik, S., Wolfson, H. J., and Nussinov, R. (2010) How does the reductase help to regulate the catalytic cycle of cytochrome P450 3A4 using the conserved water channel? *J. Phys. Chem. B* 114, 5964–5970.

(55) Oprea, T. I., Hummer, G., and Garcia, A. E. (1997) Identification of a functional water channel in cytochrome P450 enzymes. *Proc. Natl. Acad. Sci. U.S.A.* 94, 2133–2138.

(56) Guallar, V., and Olsen, B. (2006) The role of the heme propionates in heme biochemistry. *J. Inorg. Biochem.* 100, 755–760.